Astrophys Space Sci (2020) 365:11
https://doi.org/10.1007/s10509-020-3726-6

ORIGINAL ARTICLE

Real-time atmospheric extinction variation analysis with the Photometric Telescope at Xinglong Observatory

Yong Zhao[1,2] · Zhou Fan[1] · Liang Ge[1] · Juanjuan Ren[1] · Jianfeng Tian[1] · Jianfeng Wang[1] · Peng Qiu[1] · Xiaojun Jiang[1,3]

Received: 28 August 2019 / Accepted: 10 January 2020 / Published online: 15 January 2020

Abstract We present the Photometric Auxiliary System (PAS) attached to the 25-cm Photometric Telescope (PT) at Xinglong Observatory of National Astronomical Observatories, Chinese Academy of Sciences (NAOC). This PAS can provide real-time atmospheric extinction for other telescopes at the same station for flux calibration via observing standard stars, e.g. the 2.16-m reflector and 1-m telescope. Moreover, the real-time atmospheric extinction could act as a useful reference for other local telescopes regarding the adjustment of observing strategies, such as changing the exposure time, which is important for the observers. This PAS has been operated since February 2012, and we have obtained the r-band atmospheric extinction of Xinglong Observatory from February 2012 to March 2018. With these data, we have analyzed the atmospheric extinction of Xinglong Observatory in detail.

Keywords Astronomical instrumentation · Methods and techniques · Techniques: photometric

✉ Y. Zhao
zhaoyong@bao.ac.cn

Z. Fan
zfan@bao.ac.cn

1 Key Laboratory of Optical Astronomy, National Astronomical Observatories, Chinese Academy of Sciences, Beijing 100012, China

2 University of Chinese Academy of Sciences, Beijing 100049, China

3 School of Astronomy and Space Science, University of Chinese Academy of Sciences, Beijing 100049, China

1 Introduction

The precision of atmospheric extinction estimates directly affects the final photometric results, especially for flux calibration. However, most measurements of atmospheric extinction are generally carried out under photometric nights, and this quality is unavailable under the usual observational conditions, especially non-photometric nights, since the atmospheric transparency changes with location in the sky and time. Fortunately, the PAS with the PT can be used in various weather conditions, and it can provide the variation of atmospheric extinction with location in the sky and time. Thus, it is more important to provide real-time atmospheric information for other telescopes in the same observation station, especially for a sky survey and time-domain astronomy.

Detailed studies of the weather conditions at many observatories have been published previously. Taylor et al. (2004) studied the observing conditions (the sky brightness and seeing) at the Mount Graham International Observatory, which were obtained at the Vatican Advanced Technology Telescope (VATT) in U, B, V, R bands between April 1999 and December 2003. Artamonov et al. (2010) used historical data from the 1.5-m AZT-22 telescope to estimate the atmospheric extinction in V band. Sky brightness and extinction of the Mauna Kea site were studied by Walker (1983), Sayers et al. (2010), and Buton et al. (2013). Falchi (2011) employed a portable CCD camera to obtain the measurement of extinction. Ebr et al. (2015) introduced real-time atmospheric monitoring for the Cherenkov Telescope Array using a wide-field optical telescope. Sharma et al. (2017) described an Automated Extinction Monitor (AEM) for the Indian Astronomical Observatory with a commercially available telephoto lens.

Furthermore, a series of previous works that estimate the quality of observing conditions for Xinglong Observatory

(XO) have also been performed. For instance, Liu et al. (2003) and Yao et al. (2013) used data from monitoring Polaris collected from 1995 to 2001 and 2004 to 2007 by the 60/90 cm Schmidt telescope to investigate the atmospheric extinction in V band, the sky brightness, and the seeing of XO. Zhang et al. (2015) analyzed the astronomical observing conditions (the meteorology, seeing, and sky brightness) of XO from 2007 to 2014 with the Automatic Weather Station (AWS), Differential Image Motion Monitor (DIMM), and Sky Quality Meter (SQM). Zhang et al. (2016) used OMR (a spectrograph made by Optomechanics Research Inc, in Tucson, Arizona) spectra obtained by the 2.16-m reflector (Fan et al. 2016) with a wavelength coverage of 4000–7000 Å to investigate changes in the night sky from 2004 to 2015 at XO. In our work, we not only report variation of the site conditions over a longer time scale (i.e. years), but also provide real-time weather conditions for users of the XO telescopes.

Our work is organized as follows. In Sect. 2, we describe the instruments and telescope control system of the PT. Section 3 gives an introduction to the PAS with the PT. In Sect. 4, we discuss our results and present our conclusions. Finally a brief summary and conclusion are given in Sect. 5.

2 The instruments and telescope control system of PT

The Xinglong 25-cm PT is a German equatorial mount telescope (as shown in Fig. 1) at XO operated by National Astronomical Observatories, Chinese Academy of Sciences (NAOC). The XO is located ∼120 km northeast of Beijing, with an altitude of ∼960 m. The median seeing value of XO is around $1''.7$ with over one year of statistics compiled in 2014, and the sky brightness at zenith is around 21.1 mag arcsec^{-2} (V-band). More detailed information about the observing conditions of XO can be found in Zhang et al. (2015).

The PT has an effective aperture of 25 cm, and a focal ratio of f/3.8 at the Newtonian focus. The field of view of PT is $51'.4 \times 51'.4$. An Andor Zyla camera is mounted on the PT, which has fast readout speed (540 MHz and 216 MHz) mode. The filter system of the 25-cm telescope is an SDSS u, g, r, i, z broad band system. We have developed specialized software for the telescope control system, that works together automatically with the 50-cm telescope, which is at the same site as the 1-m telescope.

3 The PAS with the PT

In our work, we acquire the real-time atmospheric extinction in two steps. The first step is to calibrate the zero-point of the PT. Then, the atmospheric extinction can be obtained by fitting the atmospheric extinction formula as a function of the long term monitoring data.

Fig. 1 The 25-cm PT at Xinglong Observatory

3.1 Photometric zero-point calibration of the telescope

The following is an example of photometric zero-point calibration. The telescope photometric zero-point calibration is usually performed in photometric nights (the weather was clear and stable during the whole night). In order to do that, some suitable Landolt standards (Landolt 2013) were selected (see Table 1), which were observed on 2018 April 05. Every target was usually observed three times in each filter, and then we moved to another target. These procedures were repeated. Finally, the selected standard stars to be observed should expand to a sky coverage as large as possible. Here, we observed the standard stars in g, r and i bands with the PT.

The raw data were processed with the standard procedures for data reduction, with commands in Image Reduction and Analysis Facility (IRAF).[1] The bias and flat-field were corrected for object images with the IRAF task *ccdproc*. The IRAF task *phot* was used for aperture photometry. For most observed frames, the exposure time is ∼30s. We adopted the most suitable 2–3 times of Full Width at Half Maximum (FWHM) for aperture photometry in the frame to calculate the extinction at that time. After the photometry, we obtained the instrumental magnitudes of the standard stars. In Table 1, we listed the Landolt standard magnitudes. However, the filter bands are g, r and i. We used the SAOImage DS9[2] catalogs with the Sloan Digital Sky Survey (SDSS) Data Release (DR8) to obtain standard

[1] IRAF is distributed by the National Optical Astronomy Observatory, which is operated by the Association of Universities for Research in Astronomy, Inc. (AURA) under cooperative agreement with the National Science Foundation.

[2] http://ds9.si.edu/site/Home.html.

Table 1 Information on the Selected Landolt Standards

Star name	RA	DEC	V (mag)	$B-V$ (mag)	$U-B$ (mag)	$V-R$ (mag)	$R-I$ (mag)	V–I (mag)
SA 26-27	06:42:39.409	+44:31:47.34	10.860	+0.611	+0.113	+0.375	+0.355	+0.732
SA 26-135	06:42:58.715	+44:38:52.53	9.117	+1.110	+0.918	+0.583	+0.530	+1.113
SA 26-60	06:43:41.731	+44:30:45.40	9.542	+0.125	+0.175	+0.088	+0.069	+0.157
SA 26-95	06:45:16.159	+44:32:04.67	11.988	+0.546	+0.016	+0.326	+0.321	+0.644
SA 29-303	09:44:53.037	+44:25:07.54	8.292	+0.602	+0.174	+0.344	+0.329	+0.674
SA 29-322	09:46:31.722	+44:22:32.87	9.766	+0.488	+0.030	+0.285	+0.262	+0.560
SA 29-331	09:47:19.945	+44:24:28.55	10.001	+0.943	+0.634	+0.504	+0.475	+0.976
SA 29-251	09:47:21.715	+44:14:13.96	9.445	+0.349	−0.001	+0.219	+0.220	+0.443
SA 32-178	12:57:25.633	+44:02:02.82	11.313	+0.805	+0.463	+0.457	+0.421	+0.874
SA 32-177	12:57:17.140	+44:01:00.49	11.377	+0.601	+0.015	+0.358	+0.346	+0.706
SA 32-113	12:57:25.835	+43:56:32.95	10.834	+0.906	+0.639	+0.531	+0.461	+0.998
SA 32-212	12:56:03.313	+44:15:28.14	9.317	+1.159	+1.131	+0.609	+0.546	+1.156
SA 35-245	15:49:49.958	+44:31:19.49	7.686	+0.111	+0.101	+0.055	+0.046	+0.097
SA 35-261	15:52:04.173	+44:24:58.31	12.126	+1.508	+1.898	+0.860	+0.884	+1.740

Table 2 The coefficients, standard deviation and RMS of PT photometric system

Fliter name	Zero points (Z) (mag)	Atmospheric extinction (K) (mag)	Color term (C) (mag)	RMS (mag)
g	4.992 ± 0.015	0.269 ± 0.019	0.086 ± 0.013	0.018
r	5.090 ± 0.011	0.169 ± 0.014	0.125 ± 0.009	0.012
i	5.902 ± 0.013	0.072 ± 0.011	-0.034 ± 0.007	0.008

magnitudes in the g, r and i bands. We define the transformation equations offered by IRAF as follows,

$$g_{inst} = g_{std} + Z_g + K_g \cdot X + C_g \cdot (g-r)_{std} \quad (1)$$

$$r_{inst} = r_{std} + Z_r + K_r \cdot X + C_r \cdot (g-r)_{std} \quad (2)$$

$$i_{inst} = i_{std} + Z_i + K_i \cdot X + C_i \cdot (r-i)_{std} \quad (3)$$

where g_{inst}, r_{inst} and i_{inst} are the instrumental magnitudes, g_{std}, r_{std} and i_{std} are the standard magnitudes, Z_g, Z_r and Z_i are zero points, K_g, K_r and K_i are the first-order atmospheric extinction coefficients, C_g, C_r and C_i are the color terms in the transformation equations, and X is the airmass.

For each standard, we have obtained 21 frames for each band. Then we used the tasks *mknobsfile* and *fitparams* in IRAF to derive the parameters in (1)–(3). Table 2 lists detailed results of the photometric system of the PT, including the filter names, zero points (Z), first order atmospheric extinction (K), color terms (C) and root mean square (RMS). Figure 2 displays a comparison between the calibrated magnitudes using derived transformation coefficients and the SDSS magnitudes, which reflects the quality of our fitting. After this, we complete the zero-point calibration of the telescope. The fitted values of photometric zero points (Z) and color terms (C) will be used in the next step, i.e. calculate the real-time atmospheric extinction.

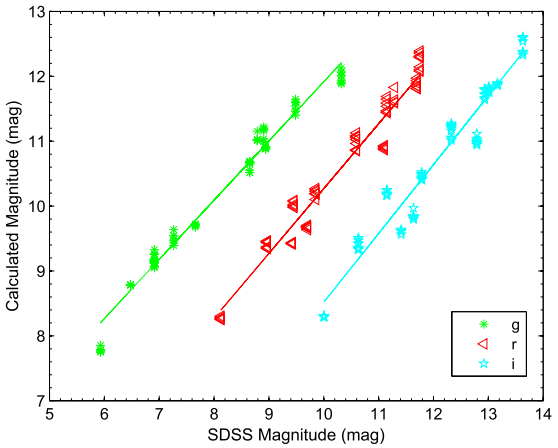

Fig. 2 The calculated magnitudes using derived transformation coefficients versus SDSS magnitudes in g, r, i band. The SDSS g and i magnitudes are shifted to -3, $+2$ magnitudes, respectively, in order to be shown clearly. The best linear fits are the solid lines

3.2 Calculate the real-time atmospheric extinction

During the observations, the telescope was pointed to certain locations in the sky to be observed, and finally obtained the photometric images. Like the procedure used for photometric zero-point calibration of the telescope, we also used

the standard procedures in IRAF to do the data reduction, and do the photometry of the standard stars in the images. Based on (1)–(3), here we change them as follows,

$$K_g = \left(g_{inst} - g_{std} - Z_g - C_g \cdot (g-r)_{std}\right)/X \quad (4)$$

$$K_r = \left(r_{inst} - r_{std} - Z_r - C_r \cdot (g-r)_{std}\right)/X \quad (5)$$

$$K_i = \left(i_{inst} - i_{std} - Z_i - C_i \cdot (r-i)_{std}\right)/X \quad (6)$$

where the zero points (Z) and the color terms (C) have been obtained in the step of photometric zero-point calibration in Sect. 3.1. Therefore, we use (4)–(6) to obtain the atmospheric extinction in each band. At present, for each image, the pipeline of the PAS used one Landolt standard star to derive the extinction of XO. Then, we calculate the average ($\overline{K}$) and variance (σ_k) of atmospheric extinctions. The average $\overline{K}$ is the atmospheric extinction value in that time period, and the variance σ_k reflects the quality of atmospheric extinction determinations. Then, we use variation of the whole night extinctions to know whether it is a photometric night.

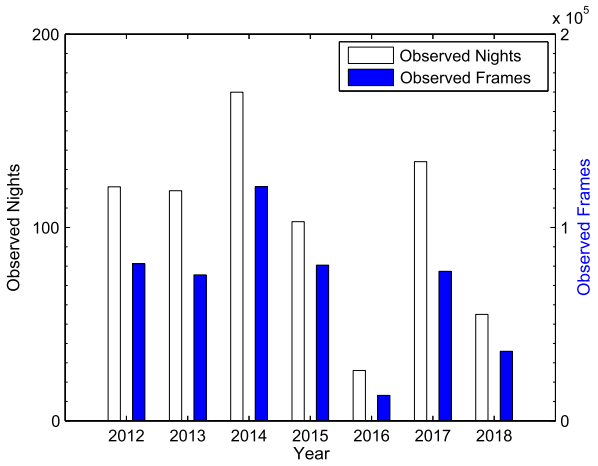

Fig. 3 The statistics of the number of observed nights and observed frames from February 2012 to March 2018 with the PT

4 The results and conclusions

The PAS described above shows how to calculate the real time atmospheric extinction with the PT. However, in the actual observations, the PT works in association with a 50-cm telescope most of the time, and does not continuously observe all the night. Therefore, the curve of the atmospheric extinction derived here is not continuous, and there are some gaps in it. For the atmospheric extinction monitoring, only the r band of the PT was used. Figure 3 shows the statistics of the number of observed nights and observed frames from February 2012 to March 2018 with the PT. From February 2012 to March 2018, we have obtained data covering more than 728 nights, which resulted in a total data size of $\sim$ 36.30 TB. As long as weather conditions allow for observations, we can observe and obtain the data, which are quite different from traditional extinction measurement. Therefore, for our long-term monitoring, both the photometric nights and non-photometric nights are available, not only at photometric nights. Usually, for each night, $\sim$ 800 frames of images were obtained.

With these data, we have analyzed the stability of PAS. Besides the photometric night of 2018 April 05, Table 3 lists the other detailed r band results of the photometric system of the PT in different photometric nights from 2012 to 2018, including the observation dates, the zero points (Z), the first order atmospheric extinction (K), the color terms (C), and the root mean square (RMS). From Table 3, we can obtain a mean value of the zero points of PAS, i.e. 5.067 ± 0.017. As shown in Table 4, we also compare the extinction value of r-band (the effective wavelength is 612.2 nm Bessell 2005) from PAS and the results from previous works about XO observational weather condition (Johnson-Cousins R-band, the effective wavelength is 640.7 nm Bessell 2005). In addition, we have compared the results of extinction of PAS with the XO 80-cm telescope (Huang et al. 2012) in the same observation nights. The results are shown in Table 5.

Figure 4 depicts an example of the atmospheric extinction curves in several stable nights, for the night with stable

Table 3 The Zero Points, Coefficients, Standard Deviation and RMS of PT Photometric System in different photometric nights from 2012 to 2018

Observation nights	Zero points (Z) (mag)	Atmospheric extinction (K) (mag)	Color term (C) (mag)	RMS (mag)
2012–05–19	5.064 ± 0.014	0.187 ± 0.011	0.143 ± 0.012	0.017
2012–07–21	5.055 ± 0.015	0.184 ± 0.015	0.146 ± 0.013	0.014
2013–07–16	5.078 ± 0.012	0.166 ± 0.016	0.131 ± 0.016	0.013
2014–10–24	5.043 ± 0.013	0.175 ± 0.014	0.145 ± 0.013	0.018
2015–09–13	5.059 ± 0.019	0.183 ± 0.018	0.122 ± 0.017	0.018
2016–10–29	5.061 ± 0.017	0.175 ± 0.014	0.126 ± 0.011	0.016
2017–09–22	5.086 ± 0.014	0.164 ± 0.013	0.131 ± 0.016	0.009
2018–02–11	5.094 ± 0.018	0.184 ± 0.013	0.125 ± 0.009	0.011
Mean	5.067 ± 0.017	0.177 ± 0.009	0.133 ± 0.010	

Table 4 The comparison between the extinction value of r-band (the effective wavelength is 612.2 nm) from PAS and the results from previous works about XO weather condition (Johnson-Cousins R-band, the effective wavelength is 640.7 nm)

Year	Filter-bands	Atmospheric extinction (K)	Reference
2012–2018	r	0.177 ± 0.009	this paper
2016	R	0.217 ± 0.019	Bai et al. (2018)
2011–2012	R	0.168 ± 0.019	Huang et al. (2012)
2008	R	0.195 ± 0.004	Zhou et al. (2009)
2006–2007	R	0.161 ± 0.008	Huang et al. (2012)
2004–2005	R	0.141 ± 0.010	Huang et al. (2012)
1998	R	0.18	Shi et al. (1998)
1995	R	0.14	Shi et al. (1998)

Table 5 Comparison between the results of extinction of PAS with the XO 80-cm telescope in the same observation nights

Observation nights	XO 80-cm	PAS
2017–09–21	0.163 ± 0.029	0.160 ± 0.019
2017–10–24	0.164 ± 0.017	0.168 ± 0.020
2017–11–19	0.171 ± 0.030	0.177 ± 0.028
2017–12–29	0.175 ± 0.004	0.180 ± 0.025
2018–01–18	0.168 ± 0.022	0.165 ± 0.035
2018–02–11	0.173 ± 0.014	0.182 ± 0.023
Mean	0.169 ± 0.005	0.172 ± 0.009

atmospheric extinction (std $<$0.07 mag). The atmospheric extinction is basically consistent during the whole night, and the value of atmospheric extinction K_r is $\sim$0.16 mag in r band. Therefore, these nights are suitable for high-precision photometric observations (photometric accuracy $<$5%). Like in Fig. 4, Fig. 5 is an example of some unstable nights, for a night with unstable atmospheric extinction (std $>$0.07 mag). As displayed in Fig. 4 and Fig. 5, for the time near twilight, the extinction value is less than that of midnight, which is consistent with the result of Lü et al. (2009). The main reason is the temperature change during the time near twilight, as described in Lü et al. (2009).

Figure 6 and Fig. 7 show the detailed variation of atmospheric extinction on a shorter time scale ($\sim$10 hours) under conditions of one stable night (photometric night, 2017 December 31) and unstable night (2018 January 5), respectively. These demonstrate more clearly how the atmospheric extinction changes over minutes. After investigating the data from these two nights, we plot the cumulative distribution of atmospheric extinction in Fig. 8. Based on the cumulative distribution of atmospheric extinction, the stable night shows a more centralized distribution than the unstable night with the mean value 0.16 mag and σ 0.03 mag in r band.

Figure 9 shows the median atmospheric extinction and its 1σ standard deviation using the data from February 2012 to March 2018 in each month. From Fig. 9, we find that the atmospheric extinction at XO changes significantly in different seasons. The best situation with the lowest atmospheric extinction occurs in October, while the worst appears in May and June when the local area suffers sand storms. These results are consistent with those in Yao et al. (2013).

Figure 10 is the statistics of the atmospheric extinction with the air temperature, relative humidity, and wind speed of the XO on a typical night of 2017 December 31. Further, similar to Fig. 9, we also compared the atmospheric extinction with the air temperature, relative humidity, and wind speed of the XO on a long time scale, from February 2012 to March 2018 in each month, which are shown in Fig. 11. From Fig. 10 and Fig. 11, we cannot find an obvious relationship between atmospheric extinction with air temperature, relative humidity, and wind speed. However, it seems that there is a trend of anti-correlation between atmospheric extinction and wind speed.

Figure 12 displays the standard deviation (SD) of atmospheric extinction from February 2012 to March 2018 and distribution on atmospheric extinction coefficients for these data. From the distribution of atmospheric extinction for these data, we concluded that about 30% of the observation times of XO are suitable for highly-precise photometric observations with extinction values less than 0.20 mag.

5 Summary

In this paper, we have presented instruments, methods and some related results of the PAS with the PT at XO. This PAS has been operated since February 2012, and we have obtained the r-band atmospheric extinction of XO from February 2012 to March 2018. From the distribution of atmospheric extinction for these data, we concluded that $\sim$30% of the observation times at XO are suitable for high-precise photometric observations.

From the results of the PAS with the PT, the atmospheric extinction at XO obtained by us manifests significant seasonal variations. The best situation with the lowest atmospheric extinction occurs in October, and the worst appears in May and June when the local area suffers serious sand

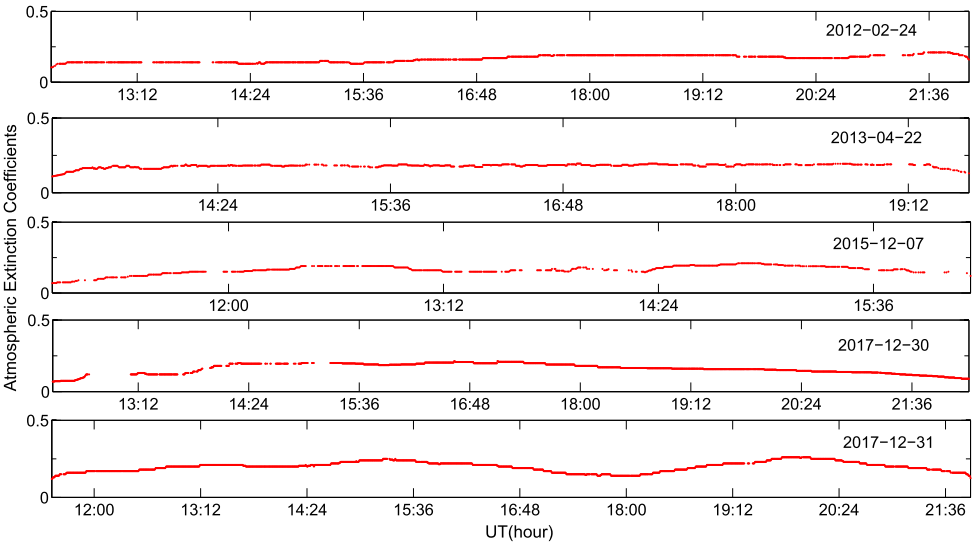

Fig. 4 An example of atmospheric extinction curves derived under some stable nights by using the data of PT

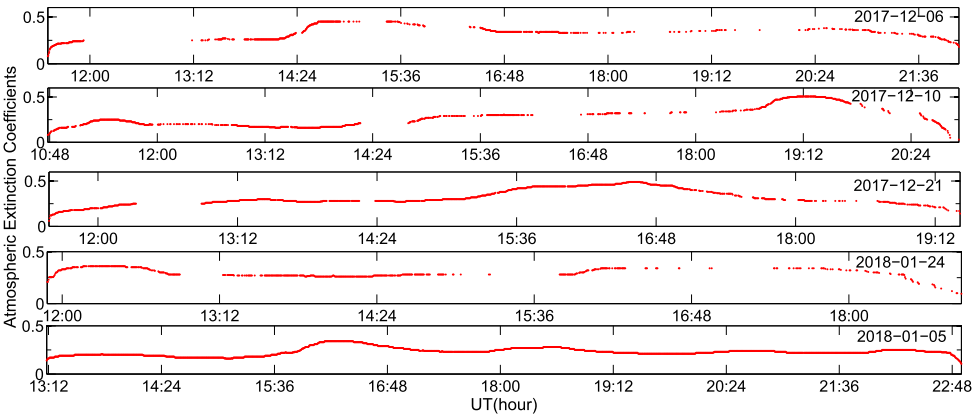

Fig. 5 Same as Fig. 4, but for some unstable nights

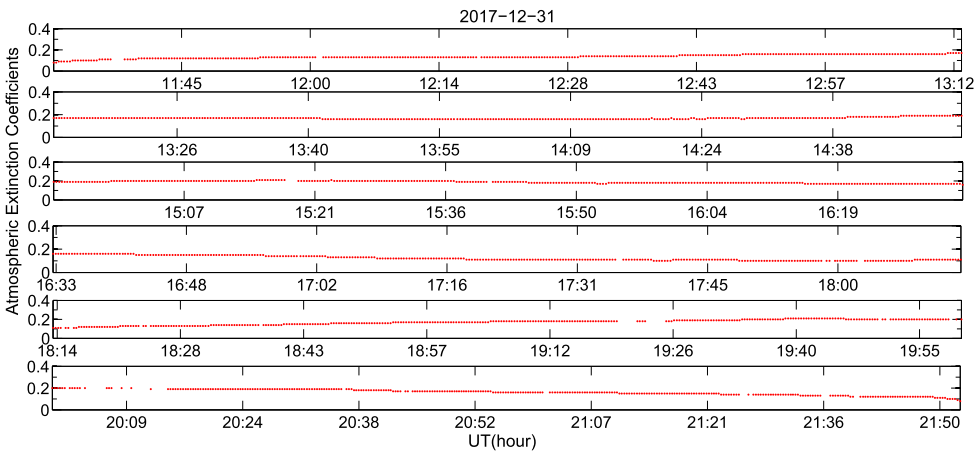

Fig. 6 An example of the variation of atmospheric extinction curves with time for one stable night (December 31, 2017) by using the data of PT

storms, which is consistent with previous works. In addition, we found that for the time near twilight, the extinction value is less than that at midnight.

The PAS is used to observe the standards and collect real-time data on the atmospheric extinction. For sky survey, you can use this to judge the weather conditions of that night, such as the Large Sky Area Multi-Object Fiber Spectroscopic Telescope (LAMOST) can use this to data correction or judge the weather conditions of that night. It is quite crucial for time-domain observations, such as for the 85-cm, 80-cm and 60-cm telescopes and other telescopes at XO. If the light curve changes, it is possible to roughly judge

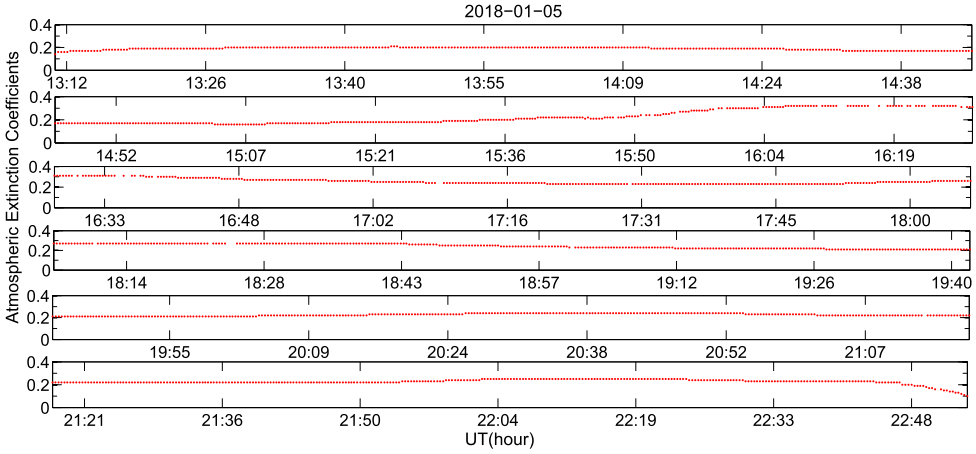

Fig. 7 Same as Fig. 6, but for one unstable night (January 5, 2018)

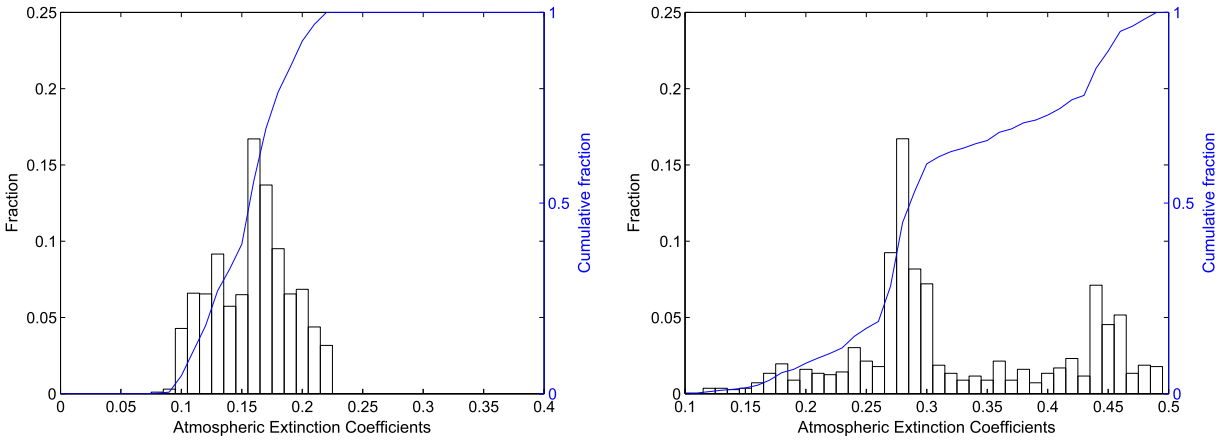

Fig. 8 The cumulative distribution of atmospheric extinction in the stable night (left panel) and in the unstable night (right panel), respectively

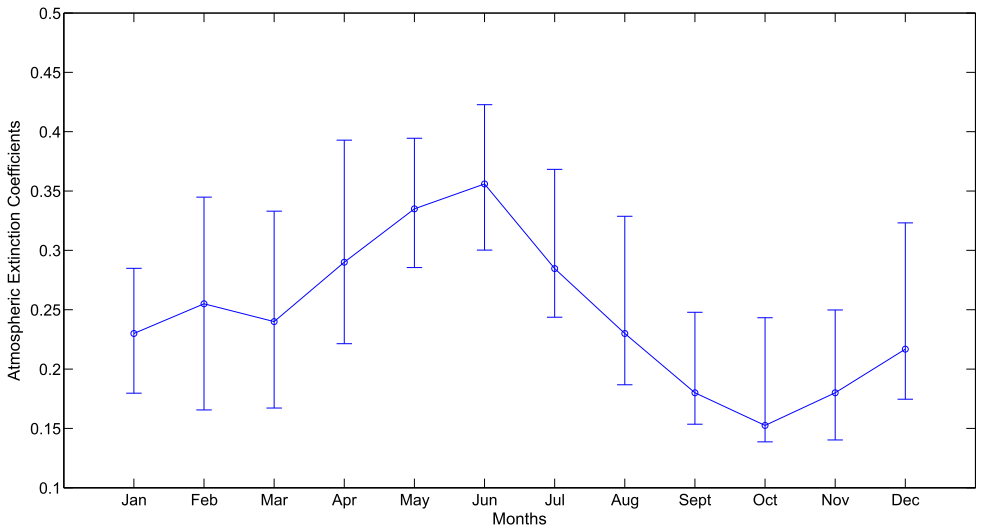

Fig. 9 The circles show the median atmospheric extinction in each month from February 2012 to March 2018 by using the data of PT. The error bar shows the 1σ standard deviation

whether the change in light curve is caused by the atmospheric extinction or not.

The monitoring of real-time atmospheric extinction is quite important for astronomical observatories, and it provides a reference to other telescopes for adjusting the observing strategies, such as changing the exposure time, which is important and useful for observers. On the other hand, the atmospheric extinction curve can reflect the long

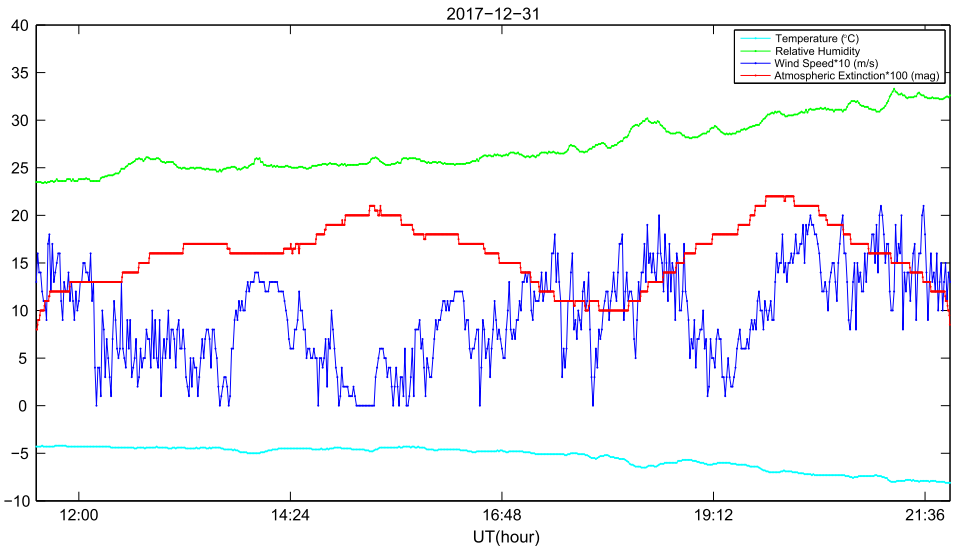

Fig. 10 Comparing the atmospheric extinction with the air temperature, relative humidity, and wind speed of the XO on a typical night of 2017 December 31. The atmospheric extinction and wind speed have been scaled by multiplying by 100 and 10, respectively, in order to be shown clearly

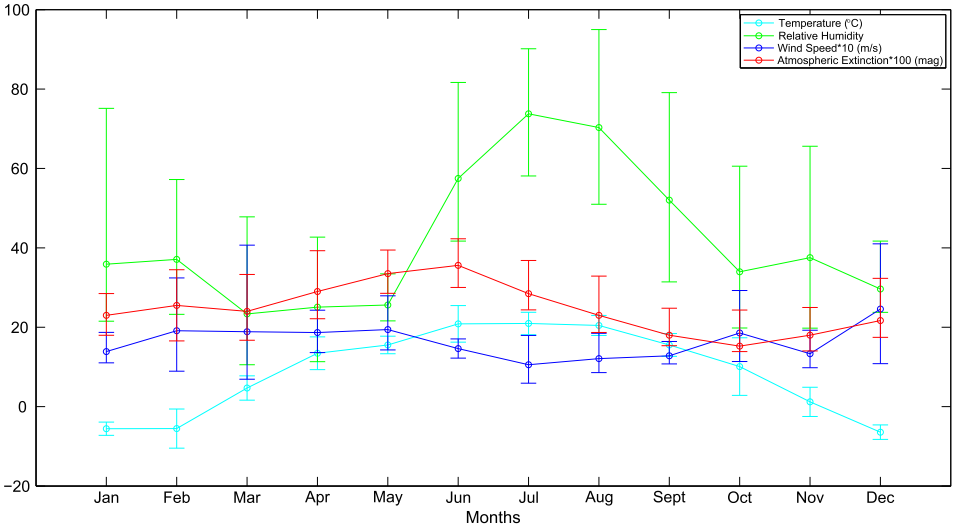

Fig. 11 Comparing the atmospheric extinction with the air temperature, relative humidity, and wind speed of the XO from February 2012 to March 2018 in each month. The atmospheric extinction and wind speed have been scaled by multiplying by 100 and 10, respectively, in order to be shown clearly

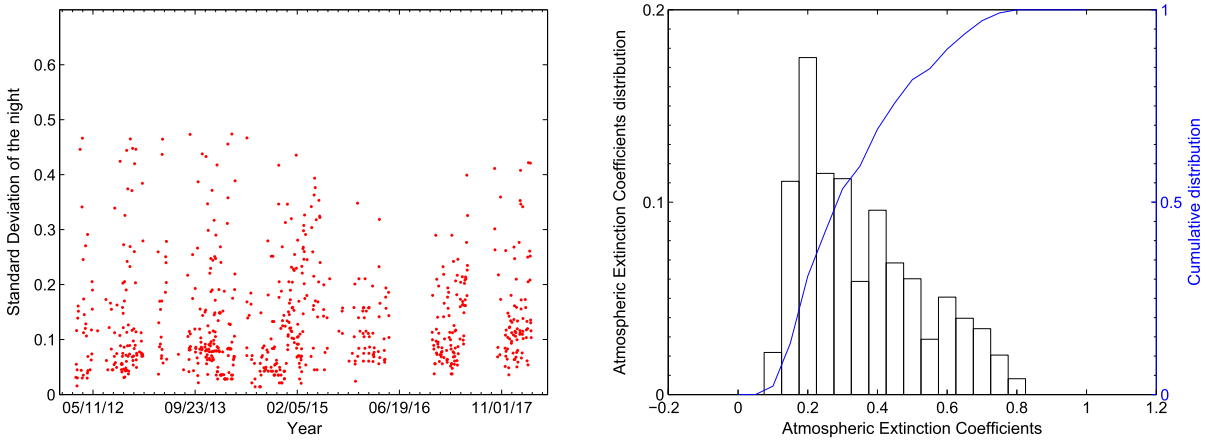

Fig. 12 The standard deviation of atmospheric extinction from February 2012 to March 2018 (left panel) by using the data of PT, and distribution of the atmospheric extinction coefficients for these data (right panel)

term variation of site conditions, not only for the purposes of monitoring, but also for scientific reference. In the next step, we will monitor the atmospheric extinction in other bands with longer time scale, which can provide more useful reference for the observations in XO. In addition, the historical and real time extinction will available to the public at our website of XO.[3]

Acknowledgements We thank the anonymous referee for his/her suggestive comments that helped improve the manuscript. This work is supported by the Open Project Program of the Key Laboratory of Optical Astronomy, National Astronomical Observatories, Chinese Academy of Sciences, the grants from Joint Research Fund in Astronomy National Natural Science Foundation of China (No. U1831209), National Program on Key Research and Development Project Grant No. 2016YFA0400804, National Key Basic Research Program of China (973 Program) No. 2015CB857002, and the National Natural Science Foundation of China (NFSC) through grants 11503045, 11373003. We also thank James Wicker, for improving the language aspects in this manuscript.

Compliance with Ethical Standards The author declares to have no conflicts of interest.

References

Artamonov, B.P., Bruevich, V.V., Gusev, A.S., et al.: Astron. Rep. **54**, 1019 (2010)
Bai, C.-H., Fu, J.-N., Li, T.-R., et al.: Res. Astron. Astrophys. **18**, 107 (2018)
Bessell, M.S.: Annu. Rev. Astron. Astrophys. **43**, 293 (2005)
Buton, C., Copin, Y., Aldering, G., et al.: Astron. Astrophys. **549**, A8 (2013)
Ebr, J., Janecek, P., Prouza, M., et al.: (2015). arXiv:1508.06798
Falchi, F.: Mon. Not. R. Astron. Soc. **412**, 33 (2011)
Fan, Z., Wang, H., Jiang, X., et al.: Publ. Astron. Soc. Pac. **128**, 115005 (2016)
Huang, F., Li, J.-Z., Wang, X.-F., et al.: Res. Astron. Astrophys. **12**, 1585 (2012)
Landolt, A.U.: Astron. J. **146**, 131 (2013)
Liu, Y., Zhou, X., Sun, W.-H., et al.: Publ. Astron. Soc. Pac. **115**, 495 (2003)
Lü, W., Zhu, W., Yuan, Ke-e., et al.: Acta Photonica Sin. **38**, 9 (2009)
Sayers, J., Golwala, S.R., Ade, P.A.R., et al.: Astrophys. J. **708**, 1674 (2010)
Sharma, T.K., Parihar, P., Banyal, R.K., et al.: Mon. Not. R. Astron. Soc. **470**, 1091 (2017)
Shi, H.-M., Qiao, Q.-Y., Hu, J.-Y., Lin, Q.: Chin. Astron. Astrophys. **22**, 245 (1998)
Taylor, V.A., Jansen, R.A., Windhorst, R.A.: Publ. Astron. Soc. Pac. **116**, 762 (2004)
Walker, M.F.: Publ. Astron. Soc. Pac. **95**, 903 (1983)
Yao, S., Zhang, H.-T., Yuan, H.-L., et al.: Res. Astron. Astrophys. **13**, 1255 (2013)
Zhang, J.-C., Ge, L., Lu, X.-M., et al.: Publ. Astron. Soc. Pac. **127**, 1292 (2015)
Zhang, J.-C., Fan, Z., Yan, J.-Z., et al.: Publ. Astron. Soc. Pac. **128**, 105004 (2016)
Zhou, A.-Y., Jiang, X.-J., Zhang, Y.-P., Wei, J.-Y.: Res. Astron. Astrophys. **9**, 349 (2009)

[3] http://www.xinglong-naoc.org/.